Synergistic Effect of Pistachio Shell Powder and Nano-Zerovalent Copper for Chromium Remediation from Aqueous Solution

Sandeep Kumar (sandeepchem83@gmail.com)
Akal University https://orcid.org/0000-0002-3969-2097
Ravinderdeep Singh Brar
AKAL UNIVERSITY
J Nagendra Babu
Central University of Punjab
Amarjeet Dahiya
Central University of Punjab
Sandip Saha
Akal University
Avneesh Kumar
Akal University

Research Article

Keywords: Zerovalent copper, Pistachio, Biomass, Cr(VI), Adsorption, Kinetics, Synergistic effect

Posted Date: May 4th, 2021

DOI: https://doi.org/10.21203/rs.3.rs-441366/v1

Version of Record: A version of this preprint was published at Environmental Science and Pollution Research on July 6th, 2021. See the published version at https://doi.org/10.1007/s11356-021-15285-4.

Synergistic Effect of Pistachio Shell Powder and Nano-Zerovalent Copper for Chromium Remediation from Aqueous Solution

Sandeep Kumar[1*], Ravinderdeep Singh Brar[1], J Nagendra Babu[2], Amarjeet Dahiya[2], Sandip Saha[1], Avneesh Kumar[3]

[1]Department of Chemistry, Akal University, Talwandi Sabo, Bathinda-151302, Punjab, INDIA

[2]Department of Chemistry, School of Basic and Applied Science, Central University of Punjab, Bathinda -151 001, Punjab, INDIA

[3]Department of Botany, Akal University, Talwandi Sabo, Bathinda-151302, Punjab, INDIA

Corresponding Author:

Email: sandeepchem83@gmail.com;

Telephone: +91-98883-3880.

Correspondence Address: Department of Chemistry, Akal University, Talwandi Sabo, Bathinda-151302, Punjab, INDIA

Abstract

Pistachio shell powder supported nano-zerovalent copper (**ZVC@PS**) material prepared by borohydride reduction, was characterized using SEM, FTIR, XRD, TGA/DTA, BET, and XPS. SEM, XRD, and XPS revealed the nano-zerovalent copper to consist of a core-shell structure with CuO shell and Cu(0) core with a particle size of 40-100 nm and spherical morphology aggregated on **PS** biomass. **ZVC@PS** was found out to contain 39% (w/w %) Cu onto the pistachio shell biomass. Batch sorption of Cr(VI) from the aqueous using **ZVC@PS** were studied, and was optimized for dose (0.1-0.5 g/L), initial Cr(VI) concentration(1-20 mg/L) and pH (2-12). Optimized conditions were 0.1 g/L doses of sorbent and pH=3 for Cr(VI) adsorption. Langmuir and Freundlich adsorption isotherm models fitted well to the adsorption behavior of **ZVC@PS** for Cr(VI) with a pseudo-second-order kinetic behavior. **ZVC@PS** (0.1g/L) exhibits q_{max} for Cr(VI) removal up to 111.1 mg/g. XPS and other spectroscopic evidence suggest the adsorption of Cr(VI) by pistachio shell powder, coupled with reductive conversion of Cr(VI) to Cr(III) by **ZVC** particles to produce a synergistic effect for the efficient remediation of Cr(VI) from aqueous medium.

Keywords: Zerovalent copper, Pistachio, Biomass, Cr(VI), Adsorption, Kinetics, Synergistic effect.

1. Introduction

Consumer demands of expanding population on the planet are met by our industries with production, which is a threat to sustainable development. Herein, industries produce goods as per the demand of the consumer. Industries meet these demands through time-efficient processes, which demand the use of chemicals that could be fossil-oriented or mining-oriented (Carvalho 2017). These chemicals then enter into the biosphere through various environmental pathways and food chains (Garvey 2019). Heavy metals are essential components of these chemicals due to their desired redox, coordination, and physical attributes (Aigberua et al. 2018; Vardhan et al. 2019). Chromium is considered as the 7th most abundant element on earth, existing in the core and mantle; and also ranked 21st in the earth crust with an average concentration of 185 mg kg^{-1} (Sperling 2005). Chromium finds anthropogenic use in leather tanning, manufacturing, electroplating, chemical refining, organic synthesis, etc. (Lunk 2015; Nigam et al. 2015; Tadesse et al. 2017). The majority of the method for the treatment of chromium in wastewater involves the use of chemical precipitation, coagulation, bioreduction, and electrocoagulation, etc. (GracePavithra et al. 2019; Owlad et al. 2009; Peng and Guo 2020; Pradhan et al. 2017). In spite of these treatment techniques, chromium does find its way into our environment, wherein it exists in two oxidation states [i.e. Cr(VI) and Cr (III)]. Trivalent chromium is relatively stable and less toxic but poses health concerns at higher concentrations. However, hexavalent chromium is very harmful even at lower concentrations due to its carcinogenicity, hemotoxicity, and genotoxicity (Barceloux and Barceloux 1999; Burrows 2019). Based on the toxicity associated with chromium, the World Health Organization (WHO) (WHO, 2003) and Bureau of Indian Standards (BIS 10500-2012) have set the permissible limit of chromium at 50 µg/L in wastewater.

The treatment of chromium in wastewater by conventional methods like coagulation, electrocoagulation, (Khan et al. 2019; Mahringer et al. 2020; Peng and Guo 2020) and chemical precipitation(Minas et al. 2017) are irreversible processes, wherein extraction of chromium in the desired form may not be feasible from the waste/sludge generated. Apart from this, conventional methods have the drawbacks of being time-consuming, require bulk wastewater, cost, and manpower intensive, poor reproducibility under variable wastewater physicochemical characteristics (Crini and Lichtfouse 2019; Hu et al. 2011; Sharma et al. 2009). More recently there have been studies on various emerging technologies for the treatment of wastewater including ion exchange (Wang et al. 2020), membrane technologies (Namdar et al. 2021), reverse osmosis (Zakmout et al. 2020), bioremediation (He et al. 2020a; Mohamed et al. 2020) phytoremediation (Kullu et al. 2020) etc. Among these techniques, adsorption is a simple and cost-effective technology. Adsorption is based upon the imbalance of intermolecular forces on the surface of solids leading the way to interaction and removal of atoms, ions, or molecules from solution onto the surface of the solid phase (Artioli 2008). Thus, adsorption is a surface phenomenon, requiring more and more active surfaces on the solid phase for efficient adsorption. Various surface-active adsorbents studied for chromium could be classified as lignocellulosic biomass (Çelebi 2020), biochar (Qu et al. 2021), zeolites (He et al. 2020b), Chitosan (Lei et al. 2020), Graphene oxide (Zhang et al. 2020), resin (Vilayatkar et al. 2020), clay (Ashour and Tony 2020), activated charcoal (Mahmudi et al. 2020; Patel 2020) etc. Among lignocellulosic biomass, Picea smithiana cone (Mittal et al. 2016), pistachio shell (Banerjee et al. 2018) etc. have been studied for chromium adsorption. These biomass have poor adsorption

and/or recovery for Cr(VI). On the other hand zeolites and activated charcoal show poor surface adsorption for Cr(VI) oxoanions, due to the characteristic electrostatic surface negative charge (Jorfi et al. 2017; Puszkarewicz and Kaleta 2019; Vaid et al. 2014).

Further, new classes of surface-active materials in the form of nanomaterials have shown promising activity. Various nanomaterials studied for Cr(VI) remediation include nZVI (Sharma et al. 2009), MnO_2 (Dinh et al. 2020), ZnO (Le et al. 2019), TiO_2 (Gopinath et al. 2020), Fe_2O_3 (Li et al. 2019), and their variants with other metal/metal oxides and chalcogenides (Karimi-Maleh et al. 2020; Peng and Guo 2020; Zhao et al. 2019). Recently Cu/Cu_2O nanoparticles have found application in electrochemical sensing (Devnani et al. 2019; Li et al. 2018) and adsorption of heavy metal (Iqbal et al. 2019). Cu/Fe bimetallic nanocomposite materials have been found suitable for remediation of Cr(VI) (Jia et al. 2019; Jiang et al. 2018; Qu et al. 2021; Zhu et al. 2016; Zhu et al. 2018), but very few literature reports are known for utilization of zerovalent copper as Cr(VI) adsorbent (Li et al. 2015a; Wu et al. 2009).

However, CuNPs tend to agglomerate during synthesis and thus the surface area and the activity of the CuNPs is reduced to a large extent (Huang et al. 2012; Li et al. 2015a; Li et al. 2015b). Thus, to prevent agglomeration, stabilizers and immobilizers can be used in-situ during the preparation of the nanoparticles, to ensure dispersion of the nanoparticles. The use of dispersing agents not only provides stable support to the nanoparticles, but also solves the problem pertaining to agglomeration of nanoparticles resulting in pressure drop in the reactor bed and also to the recyclability of nanoparticles (Wu et al., 2009). Supporting materials such as polymers (Saraswathi et al. 2019), zeolites (Xu et al. 2018a), clay (Pandey and Saini 2019), graphene (Xu et al. 2018b), etc. has been widely utilized for the synthesis of adhered nanoparticle scaffolds. Immobilizers have the added advantage of easy separation of the material from the water/wastewater system. The selection of material to be used as an immobilizer becomes very important. As the material must not themselves act as secondary pollutants after they have been employed for the removal of primary pollutants. Many reports support the use of agricultural byproducts and wastes for the removal of heavy metals from wastewater. These biodegradable adsorbent materials are significant in terms of their low cost, abundant availability, easy disposal and use as green adsorbent without pre-treatments with chemicals (Afroze and Sen 2018). Therefore, the use of biodegradable materials as immobilizers becomes very important for this field of application (Guerra et al. 2018). Earlier one of the authors (Sharma et al. 2018; Sharma et al. 2015) has reported the role of cellulose as an immobilizer and in nZVI reductive regenerative for enhanced adsorption of chromium. Thus, lignocellulosic materials can stabilize metal nanoparticles and enhance the adsorption of Cr(VI). Therefore, this study attempted to use pistachio shell powder, a biodegradable material known for its Cr(VI) removal tendencies (Banerjee et al. 2018) as support for the synthesis of zero-valent copper nanoparticle dispersed nanocomposite material using appropriate chemical reduction methods and investigate the synergistic effect of these two adsorbents for their Cr(VI) removal efficacies.

2. Materials and Methods

2.1 Preparation of pistachio shell (PS) powder

Waste pistachio shells used for the studies were collected from the local market. The pistachio shells were washed twice with distilled water before subjecting to air drying in an electric oven for the duration of 24 h at 100 ^{o}C temperature. The dried shells were grounded using a common household grinder (Bajaj GX1) and sieved to get a homogenous mesh of opening size 250 -350 µm.

2.2 Reagents and material

The chemical reagents used for the studies including $CuSO_4.5H_2O$, $NaBH_4$, $K_2Cr_2O_7$, diphenylcarbazide were analytical reagent grade and purchased from Loba Chemie Laboratory Reagents, India. All reagents were prepared in deionized water. Diphenylcarbazide was used for the determination of Cr(VI) concentrations (Lace et al. 2019).

2.3 Preparation of ZVC@PS composite

Pistachio shell powder (4.0 g) was suspended in 100 mL of distilled water at room temperature. $CuSO_4.5H_2O$ (0.17 mol, 4.4 g) solution in 50 mL water was added to the reaction mixture with vigorous stirring. To this solution was added dropwise a 20% aqueous $NaBH_4$ solution (100 mL) at a constant rate of 1 mL/min. After the completion of the addition, the reaction mixture turned black and was subjected to stirring at room temperature for 30 min. The black material was filtered, washed with an excess amount of distilled water followed by methanol, and dried under inert conditions *in vacuo*.

2.4 Physical Characterization of ZVC@PS

FTIR analysis (Bruker, Model: Tensor 27) was performed to determine the characteristic bonds in **ZVC@PS**. X-ray powder diffraction analysis (Bruker, Model: D8-Advance) was performed to evaluate the crystal structure and crystal phase of the **ZVC@PS** composite at 2θ angles ranging from 5^{o} to 80^{o} with a scanning rate of 3^{o} (2θ) per minute at an accelerating voltage of 40 kV and emission current of 40 mA. The surface morphologies of the **ZVC@PS** and pistachio shell powder were characterized by field emission scanning electron microscopy (FESEM, Carl Zeiss, Model: Merlin Compact, Germany) with integrated energy dispersive X-ray (EDX) analyzer system. X-ray Photo-electron spectroscopy (XPS, Physical Electronics, Model: PHI 5000 VersaProbe III, USA) was used to determine the main element composition and valence state changes of the **ZVC@PS** composite. Pistachio shell powder and **ZVC@PS** specific surface area were investigated in BET (Micromeritics, Model: ASAP 2010, France) at -196 ^{o}C. Adsorbent degassing was performed under a nitrogen environment at 150 ^{o}C temperature for 4 h. Thermogravimetric measurements were performed using Thermogravimetric/Differential Thermal Analyzer (EXSTAR SII 6300, LabX, Canada) at a heating rate of 10 ^{o}C/min. UV-vis spectrophotometer (Shimadzu Japan, Model: UV-2450) was used for determination of Cr(VI) concentration using diphenylcarbazide method.

2.5 Experimental

2.5.1 Adsorption Equilibrium Study

A stock solution (1.0 mM) of $K_2Cr_2O_7$ (294.0 mg) was prepared by dissolving it into deionized water (1000 mL) and standard Cr(VI) concentrations of 2-20 mg/L obtained by serial dilution of the stock solution with deionized water, were used for the adsorption study. **ZVC@PS** (100 mg/L) was added to individual Erlenmeyer flasks containing 100 mL solutions of Cr(VI) (2-20 mg/L), and the resulting mixtures were incubated at 25 ± 2 ºC and 180 rpm for 24 h. The samples were subjected to filtration using Whatman 1 filter paper and analyzed for Cr(VI) concentration via diphenylcarbazide method using UV-Vis spectrophotometer at a wavelength of 540 nm (Lace, Ryan et al. 2019). The absorption efficiency (i.e. % Cr removal) and equilibrium adsorption capacity, q_e ($mg_{Cr(VI)}/g_{\mathbf{ZVC@PS}}$) were calculated using equation (1) and (2).

$$\text{Cr(VI) removal } (\%) = \frac{C_o - C_e}{C_o} \times 100 \quad (1)$$

Where, C_o and C_e ($mg{\cdot}L^{-1}$) are the initial and equilibrium Cr(VI) concentration in mg/L, respectively.

$$q_e = \frac{(C_o - C_e)V}{W} \quad (2)$$

Where V is the volume of the solution (in L) and W is the mass of adsorbent **ZVC@PS** taken.

Studies were performed by varying parameters like pH, adsorbent concentration, and initial dichromate concentration to investigate the effect of different experimental parameters on the Cr(VI) adsorption and under optimized conditions. The Cr(VI) concentration of 20 mg/L and **ZVC@PS** dose concentration of 1.0 g/L was selected for pH optimization study. Cr(VI) solutions (100 mL) having different pH ranging from 2 to 10 were prepared by adjusting the pH with 1N HCl and or NaOH solutions. The optimum dose determination experiment was performed using 20 mg/L of Cr(VI) solution with varying amounts of **ZVC@PS** (0.05, 0.1, 0.15, and 0.2 g/L) at optimum pH 3. All experiments were carried out in duplicate and average results are reported.

2.5.2 Kinetic and isotherm experiments

Adsorption of Cr(VI) using **ZVC@PS** was analyzed for its kinetics of adsorption and for optimization of equilibration time. The procedure used to perform kinetic experiments was the same for the determination of adsorption efficiency of **ZVC@PS**. To a 100 mL solution of Cr(VI) at a concentration of 20 mg/L was added 10 mg of **ZVC@PS** and incubated at 25 ± 2 ºC and 180 rpm for 24 h. A fixed volume of the reaction mixture was withdrawn and diluted at regular intervals of time i.e. 0.5, 1, 2, 3, 4, 6, 8, 10, 12, and 24 hr to analyze the residual Cr(VI) concentration. The data thus obtained for Cr(VI) adsorption onto **ZVC@PS** as a function of time and was plotted to find the suitable fit to kinetic model.

2.5.3 Adsorption isotherm study

The adsorption equilibriums were determined using Langmuir and Freundlich isotherms between **ZVC@PS** and Cr. In Langmuir adsorption isotherm, adsorption is assumed to be independent for each entity of adsorbate with the formation of a monolayer on the surface. Linearized form of the Langmuir equation (3) is:

$$\frac{1}{q_e} = \frac{1}{q_{max} K_L C_e} + \frac{1}{q_{max}} \quad (3)$$

This model was used to draw a correlation between q_e (mg/g) i.e. the amount of Cr(VI) adsorbed at equilibrium, C_e (mg/L) i.e. equilibrium solute concentration, where q_{max} is the maximum saturation monolayer adsorption expressed in mg/g, and K_L is the Langmuir equilibrium constant.

The equilibrium parameter in Langmuir isotherm can be expressed in terms of a dimensionless constant (R_L, also called separation factor) by equation (4) as follows:

$$R_L = 1/(1 + K_L C_0) \quad (4)$$

The value of R_L signifies the nature of isotherm i.e. unfavorable for $R_L > 1$; linear for $R_L = 1$; favorable for $0 < R_L < 1$; or irreversible for $R_L = 0$.

The Freundlich adsorption isotherm is applied to non-ideal sorption on heterogeneous surfaces as well as multilayer sorption and adsorption capacity is related to the Cr(VI) concentration at equilibrium. Linear form of Freundlich model is defined by equation (5) as:

$$\log q_e = \log K_f + \frac{1}{n} \log C_e \quad (5)$$

A straight-line graph is obtained upon plotting *log* q_e versus *log* C_e with a slope of $\left(\frac{1}{n}\right)$ and intercept log K_f. The adsorption capacity and adsorption intensity are related to Freundlich constant K_f and $\left(\frac{1}{n}\right)$,respectively.

2.5.4 Removal Kinetics study

Adsorption kinetics depends upon various factors such as initial concentration, contact time, and temperature. The Cr(VI) adsorption kinetic studies are performed with 20 mg/L of Cr(VI) aqueous solution and 100 mg/L of adsorbent **ZVC@PS**.

The pseudo-first-order and pseudo-second-order kinetic models are used for the investigation of the mechanism of reduction, mass transport, and chemical reaction process involved in adsorption of Cr(VI) by **ZVC@PS**.

Linearized form of pseudo-first-order model is as given in eqn (6)

$$\ln (q_e - q_t) = \ln q_e - K_t \quad (6)$$

where; q_e = amount of chromium adsorbed at an equilibrium in (mg/g)

q_t = amount of chromium adsorbed at time t

K = rate constant

Linearized form of pseudo-second-order is as given in eqn (6):

$$\frac{t}{q_t} = \frac{1}{K_p q_e^2} + \frac{t}{q_e} \quad (6)$$

where, K_p is pseudo-second-order rate constant.

3. Result and discussion

3.1 Characterizations of ZVC@PS

3.1.1 XRD Pattern Analysis

X-ray powder diffraction patterns of **ZVC@PS** before and after Cr adsorption are shown in Fig. 1. XRD of **ZVC@PS** contained peaks (2θ) at 22.1, 36.5, 43.2, 50.4, 61.3, and 74.1°. The peaks (2θ) at 43.2, 50.4, and 74.1° are assigned to characteristic peaks of zerovalent copper (JCPDS 89-2838) (Ismail 2020). Two peaks (2θ) observed at 36.5 and 61.3° were ascribed to the presence of Cu_2O (JCPDS-05-0667) as a minor component along with Cu(0) (Huang et al. 2012). The diffraction peak (2θ) at 22.1° in **ZVC@PS** is attributed to the typical reflection plane (002) of the lignocellulose framework of pistachio shell powder used as support material (JCPDS card no. 03-0289) (Cottayil et al. 2015). The XRD pattern adsorbent (**Cr-ZVC@PS**) exhibited the disappearance of peaks characteristic of Cu(0) nanoparticles at 43.2, 50.4, and 74.1° upon Cr(VI) adsorption at pH 3. This is ascribed to oxidation of Cu(0) to Cu(I or II) during reductive removal of Cr(VI) to Cr (III).

3.1.2 FTIR spectral Analysis

Fourier Transform Infrared (FTIR) spectral analysis was employed for the determination of characteristic bonds in the lignocellulosic biomass containing pistachio shell powder and immobilized zerovalent copper on pistachio shell powder as a nanocomposite material. The pistachio shell powder with the presence of lignocellulose biomass was characterized by FTIR. The IR of **PS** showed absorption bands at 3390, 2918, 1632, 1384, 1178, 1161, 1139, 1084, and 877 cm^{-1} (**Fig. 2**). The bands that appeared at 1178, 1161, 1084, and 877 cm^{-1}, for the **PS**, were characteristic of the monomer pyranose ring structure of cellulose. The broad peak at 3390 cm^{-1} was assigned to -OH stretching vibrations of primary/secondary -OH groups of the glucopyranose of cellulose or phenolic -OH groups of lignin present as a basic framework of biomass. The peak at 2917 cm^{-1} is attributed to aliphatic C–H stretching, which confirmed the presence of CH_2/CH_3 groups, however, the band at 1380 cm^{-1} is characteristic of the bending of the C–H group (Liu et al. 2006). The absorption band at 1632 cm^{-1} was attributed to the bending mode of the absorbed water. The peaks at 1084 and 877 cm^{-1}, respectively, correspond to the C–O–C group of primary hydroxyl stretching at C_6 and C_1-H group deforming with ring vibration. This confirms the β-glycosidic linkage (Banerjee et al. 2018). The surface chemical interaction of zerovalent copper with the functional groups of the lignocellulose framework of pistachio biomass was evident from the significant shifts in all absorption peaks. The reductive adsorption of chromium on **ZVC@PS** changes the chemical nature of **ZVC** particles on the surface and hence results in its decreased interaction with the functional groups causing the shift of bands towards normal values as appeared in FTIR of pistachio shell powder.

3.1.3 FESEM and EDX Analysis

The morphologies of the synthesized **ZVC@PS** nanocomposite material were analyzed using a field emission scanning electron microscope (FESEM). The pistachio shell powder exhibited undefined morphologies with particle sizes ranging from 10 to 100 µm as shown in **Fig. 3a**. FESEM of zero-valent copper (ZVC) particles (**Fig. 3b**), synthesized by borohydride reduction, were found primarily in an agglomerated state but well dispersed on the

surface of the pistachio shell powder. The Cu^0 nanoparticles were spherical in shape (**Fig. 3c**) and were formed with an average size of 40 nm. The SEM-EDX spectrum analysis of **PS** contains peaks from carbon and oxygen. The EDX spectrum of **ZVC@PS** exhibits peaks from copper along with carbon and oxygen, with no contamination from any other metal. The adsorption of Cr(VI) on **ZVC@PS** was confirmed from the appearance of the characteristic peak of Cr along with other elements (**Fig. 3d-f**).

3.1.4 BET Analysis

Brunauer-Emmett-Teller (BET) analysis of **ZVC@PS** was performed and compared with **PS** to determine the surface area and contribution of immobilized nano-zerovalent copper (**ZVC**) towards the surface area of the material. The specific surface area of **PS** was found to be 0.483 m^2/g with an average BJH (Barrett-Joyner-Halenda) pore size distribution of 5.7578 nm (Turan and Mesci 2011). The relatively lower surface area suggests the microporous nature of the **PS**. Further, it characterized the poor adsorption capacity of **PS** for Cr(VI) up to 28 mg/g (Banerjee et al. 2018). On the contrary, the specific surface area of the **ZVC@PS** was found to be 5.84 m^2/g, which was significantly higher than that of **PS**. The average BJH pore diameter of **ZVC@PS** was observed at 911 nm with the satellite peak at 1374 nm (**Fig. 4b**). The substantial increase in specific surface area of **ZVC@PS** was attributed to additional pores created by immobilized nano zerovalent copper (**ZVC**) on the surface of **PS**.

3.1.5 XPS Analysis

X-ray photoelectron spectroscopy (XPS) was used to determine the elemental compositions of surfaces of **ZVC@PS** and Cr(VI) adsorbed **ZVC@PS**. The XPS survey scan of **ZVC@PS** and Cr(VI) adsorbed **ZVC@PS** is depicted in **Fig. 5a**. Further, the deconvolution of the data was carried out with curve smoothing for Cu 2p and O1s to find out the various source and oxidation states of these elements. The analysis of the survey scan of **ZVC@PS** showed characteristic peaks in the range 529-536, 823, and 930-960 eV, which is characteristic of elements O, C, and Cu, respectively in the sample surface.

The binding energy peaks for Cu 2p of **ZVC@PS** were observed at 932.1, 934.3, 942.5, and 953.4 eV (**Fig. 5b**). These peaks were deconvoluted to find the contribution of various Cu species. The binding energy peak at 932.1 and 953.4 eV suggest the presence of Cu(0) whereas, the binding energy peak at 934.3 and 942.5 eV are characteristic of Cu(II) present in **ZVC@PS** (Chang et al. 2019; Dong et al. 2014; Wu et al. 2009). The analysis of binding energy of Cu in **ZVC@PS** indicates the presence of Cu in Cu(0), as well as Cu(II) on the surface, wherein surface-Cu(II), could be attributed to the chemisorbed impurities of oxygen species. The **Fig. 5d** is the O1s XPS spectrum of **ZVC@PS** that has three different peaks at 529.4, 531.1, and 532.4 eV, which are attributed to Cu(I) oxide, oxygen in biomass polymer, and chemisorbed oxygen species like O, ^{-}OH, etc., respectively (Wang et al. 2015).

The Cr(VI) adsorbed **ZVC@PS** showed peaks at 529-534, 570-590, 823, and 930-960 eV, are characteristic of elements O, Cr, C, and Cu, respectively. Upon deconvolution of O1s spectral peak from 529-534 eV, showed the presence of only two species in the sample characterized by the peak at 529.5 and 531.4 eV. The O1s peak at 532.4 is attributed to the C=O, C-O, of biomass as well as the Cu_2O due to sorption of Cr(VI). The characteristic

deconvoluted peak corresponding to O1s at 534.4 eV in **ZVC@PS** was missing in the Cr(VI) adsorbed sample and could be attributed to the displacement of chemisorbed oxygen by the incoming Cr(III/VI) species on the surface of **ZVC**. The weak $Cr2p_{3/2}$ and $Cr2p_{1/2}$ binding energy peaks observed at 574 and 585 eV, respectively, were characteristic of Cr(III) oxide and $Cr(OH)_3$. Thus indicating reduction of Cr(VI) to Cr(III) under the adsorption conditions using **ZVC@PS** as adsorbent. The binding energy peak of Cu in Cr(VI) adsorbed **ZVC@PS** showed four deconvoluted peaks at 931, 933, 942.2, and 951.8 eV. The presence of CuO in Cr(VI) adsorbed **ZVC@PS** was characterized by the Cu $2p_{3/2}$ and Cu $2p_{1/2}$ at 933.6 and 951.8 eV, respectively (Chang et al. 2019; Ji et al. 2018; Park et al. 2006; Wang et al. 2015). The Cu 2p peaks after Cr(VI) adsorption showed a shift to lower binding energies as it was attributed to the lower concentration of Cu(II) species after Cr(VI) adsorption.

3.1.6 TGA Analysis

Thermal stabilities of pistachio shell powder (**PS**), zerovalent copper loaded pistachio shell powder nanocomposite before (**ZVC@PS**) and after chromium adsorption (**ZVC@PS-Cr**) were studied by TGA and DTA techniques. In **Fig. 6a**, the **PS** decomposed completely in TGA analysis, as it consists of only organic matters. The TGA curve of **ZVC@PS** showed mass loss up to 60% at the temperature 410 °C and retained the remaining mass up to 600 °C. The TGA curve of **ZVC@PS** after Cr adsorption showed higher mass loss up to 80% till 410 °C and no further mass loss observed till 600 °C. This trend of TGA curves indicates the presence of non-oxidizable inorganic substances in **ZVC@PS** and **ZVC@PS-Cr** materials that did not decompose till 600 °C. The DTA curves of **PS**, **ZVC@PS**, and **ZVC@PS-Cr** are shown in **Fig. 6b**. All three materials exhibited thermal degradation in two stages. The first stage or primary decomposition having a temperature range from 220-320 °C involves the weight loss of 65% with degradation of glycosyl units of hemicellulose and cellulose accompanied by the evolution of gases like CO, CO_2, H_2O, etc. along with the formation of levoglucosan and charred residues (Shafizadeh 1982). The second stage or secondary decomposition with a temperature range from 340-500 °C was assigned to degradation of levoglucosan, decomposition of high energy bonds of lignin, and burning of char, resulting in loss of 30% of total weight (Cheng et al. 2012). In **ZVC@PS** the thermal decomposition was observed in the temperature range of 200-290 °C in the first stage and 310-400 °C in the second stage. The shift in the degradation curve towards the lower temperature in **ZVC@PS** indicated the copper-mediated internal oxidative combustion of lignocellulosic biomass resulting in its lower thermal stability in comparison to **PS**. There was no significant change observed in the decomposition curve up to 600 °C, which indicates the complete oxidation of Cu(0) to Cu(II). The TG curve of the chromium adsorbed sample exhibited a shift towards higher temperature in comparison to **ZVC@PS**, but with a narrow decomposition temperature range between 270-300 °C in the first stage and 310-370 °C in the second stage. The residual content was significantly higher than **PS** in before and after Cr(VI) adsorption samples of **ZVC@PS**, which accounted for oxidation of copper and adsorption of Cr(VI).

The two thermal decomposition peaks at 320 °C and 480 °C were observed in the first derivative (DTA) curve of **PS** pyrolysis. The two decomposition peaks were ascribed to the loss of two structural components of the lignocellulose framework i.e. primary decomposition of relatively simpler cellulose structure and secondary decomposition of

highly complex lignin structure with high-energy bonds. In the case of copper-loaded **ZVC@PS**, two endothermic peaks were observed at 285 and 380 ºC, with significant lower temperature shifts of 35 K and 100 K, in the primary and secondary decomposition curves, respectively in comparison to **PS**. The agglomeration of copper on the surface of **PS** prevents the oxidation of cellulose and results in more heat gain in **ZVC@PS**. Further, the narrowing of heat gain peaks in the case of **ZVC@PS** suggested the heat mediated conversion of copper to its oxide resulted in heat loss, which reinforced the overall degradation process. However, in Cr(VI) adsorbed samples, the presence of oxides of copper and chromium further prevents cellulose oxidation and results in a high-intensity endothermic peak with a slight shift (15 K) of the primary decomposition curve towards the higher temperature in comparison to **ZVC@PS**.

3.2 Adsorption Studies

3.2.1 Effect of pH on Cr (VI) adsorption

The pH of a solution plays a regulatory role in the adsorption of oxoanion like Cr(VI). Therefore, the pH of the solution was optimized for the adsorption of Cr(VI) onto **ZVC@PC**. The adsorption studies were performed in varying pH conditions from 2 to 10 with **ZVC@PS** dose of 100 mg/L and Cr(VI) concentration of 20 mg/L. As the pH increased from 2 to 10, the Cr(VI) uptake efficiency of **ZVC@PC** was decreased from 100 mg/g to 10 mg/g (**Fig. 7**). The adsorption under pH 2 and 3 showed similar results, however, under highly acidic conditions of pH 2, the solution turned yellowish due to dissolution of the oxidized Cu into the solution. Dissolution of Cu(I/II) from **ZVC@PS** was restricted upon increasing the pH to 3 and above. The higher removal efficiency for Cr(VI) at lower pH conditions is ascribed to: (a) surface protonation of **ZVC@PS** resulting in positively charged surface favoring attractive interaction with Cr(VI) oxoanion; (b) protonation of Cr(VI) to reduce electrostatic repulsions with the surface of **ZVC@PS** and thus facilitates the overall reductive removal of Cr(VI) ions. At higher pH, the proton concentration is diminished and the negative charge on Cr(VI) is electrostatically less favored for adsorption on the **ZVC@PS** surface.

*3.2.2 Effect of **ZVC@PS** dose on Cr(VI) adsorption*

Effect of adsorbent dose of **ZVC@PS** was investigated by changing the adsorbent dose from 50 to 200 mg/L with a 20 mg/L Cr(VI) solution maintained at pH 3. As the adsorbent dose of ZVC@PC increased from 50 to 200 mg/L, the removal of Cr(VI) increased from 20 to 70% (Fig. 8). This may account for the increase in the number of available adsorption sites on the nanocomposite adsorbent with the increase in adsorbent dose, resulting in the significant adsorptive removal of Cr(VI) from the solution. As the dose of the adsorbent was increased from the Cr(VI) adsorption (q_e) decreased from 73.22 mg/g to 58.13 mg/g. There was a marginal change in q_e from 100 mg/L to 150 mg/g followed by a decrease in adsorption at 200 mg/g. dose of adsorbent can be attributed to the decrease in the number of Cr(VI) ions available per unit mass of the adsorbent at higher adsorbent dose. Consequently, the active sites on the adsorbent surface remained unsaturated in higher doses. Thus for the optimized conditions used for further study is the adsorbent dose of 100 mg/L.

*3.2.3 Effect of Cr(VI) concentration on adsorption by **ZVC@PS** and Adsorption Isotherms*

Cr(VI) ion uptake equilibrium under varying initial concentration of Cr(VI) (1-20 mg/L) were studied. The Cr(VI) uptake increased from 9.42 to 99.3 mg/g, upon increasing the concentration of an aqueous solution from 1 to 20 mg/L. However, the percentage removal decreased from 100% to 53.17% upon increasing the initial concentration of Cr(VI). These results could be attributed to the increase in the number of Cr(VI) competing for the same amount of absorbent under increased initial concentration (**Fig. 9**).

The equilibrium data fitted to both Langmuir and Freundlich adsorption isotherm models and it confirmed the monolayer adsorption behavior of **ZVC@PS** for Cr(VI) adsorption from aqueous solution (**Fig. 10**). The value of q_{max}, adsorption energy (K_L), and dimensionless factor R_L determined from a linear fit diagram of Langmuir adsorption isotherm models were 111.11 mg/g 1.5 L/mg, and 0.667, respectively (**Table 1**). As the value of R_L lies between 0 and 1, indicates favorable adsorption of Cr(VI) on **ZVC@PS**.

3.3 Kinetic equilibrium study

The rate of Cr(VI) adsorption was slow with the removal of 77.50% of Cr(VI) during the first 120 minutes. The Cr(VI) adsorption further increased from 77.50% up to 93.50% in 17 hrs. The initial increase in the adsorption could be attributed to the free availability of adsorption sites on the surface of the adsorbent. Further, the slow kinetics could be attributed to the diffusion of the anion to the surface of the **ZVC@PS** in the pores.

Lagergren pseudo-first-order and pseudo-second-order adsorption kinetic models were applied to the data. The linear fit diagram of pseudo-first order and pseudo-second-order adsorption kinetic plot are presented in **Fig. 11a-b**. The kinetic plot shows a poor fit to pseudo-first-order kinetics with R^2 equal to 0.805, whereas a good fit with pseudo-second-order kinetics with R^2 equal to 0.989 further verified with a significant chi-square value at a 95% confidence level. The q_{max} and K_t for the adsorption under pseudo-second-order kinetic fit is 83.3 mg/g and 1.618×10^{-3} min^{-1}.

4. Discussion

The adsorption experiments showed that the Cr(VI) adsorption capacity (111.1 mg/g) of nano zerovalent copper immobilized on to pistachio shell powder (**ZVC@PS**) was significantly higher than pistachio shell powder (27.95 mg/g) (Banerjee et al. 2018), polymer foam (PEI-PAA) immobilized zero-valent copper (3.77 mg/g) (Li et al. 2015a) and immobilized zerovalent Fe(0) (50 mg/g) used for the treatment of Cr(VI) from wastewater(Shi et al. 2011) (**Table 2**). This higher Cr(VI) adsorption efficiency of **ZVC@PS** may be ascribed to the formation of well-dispersed **ZVC** nanoparticles on the surface of pistachio shell powder during synthesis, which otherwise gets agglomerated in the absence of support. A synergistic effect was observed between the Cr(VI) adsorption tendency of pistachio shell powder and reductive removal of Cr(VI) by zero-valent copper, which causes a significant increase in Cr(VI) removal efficiencies of **ZVC@PS**. The optimum pH for the Cr(VI) adsorption studies with **ZVC@PS** was in the acidic conditions, thus favoring its attractive interaction with Cr(VI) oxoanion. The removal of Cr(VI) was improved with increasing the dose of **ZVC@PS**, which was ascribed to an increase in the available adsorption sites

in the nanocomposite. Langmuir and Freundlich adsorption isotherm models confirmed the monolayer adsorption behavior of **ZVC@PS** for Cr(VI). **ZVC@PS** nanocomposite followed pseudo-second-order kinetic for the Cr(VI) adsorption with a significant R^2 value of 0.989.

Conclusion

ZVC@PS an eco-efficient nanocomposite was synthesized, characterized, and used for the removal of Cr(VI) from aqueous solution. Batch experiment studies demonstrated that Cr(VI) removal rate was increased with a decrease in pH and initial Cr(VI) concentration, and increase in **ZVC@PS** dose. At optimum conditions, the Cr(VI) removal capacity of **ZVC@PS** is observed as 111.1 mg/g, and the normalized adsorption efficiency of Cu for Cr(VI) in **ZVC@PS** is 284.84 mg/g, which is quite significant. The mechanism of removal of Cr(VI) by **ZVC@PS** was investigated as surface adsorption with concomitant reduction of Cr(VI) to Cr(III). In conclusion, the pistachio shell powder immobilized zerovalent copper could be an efficient and promising material for Cr(VI) remediation from an aqueous medium.

Abbreviations

PS: pistachio shell; ZVC: zerovalent copper; SEM: scanning electron microscopy; EDX: Energy Dispersive X-rays; FTIR: Fourier-transform infrared; XRD: X-ray powder diffraction; TGA: thermo-gravimetric analysis; DTA: differential thermal analysis; BET: Brunauer–Emmett–Teller; BJH: Barrett-Joyner-Halenda; XPS: X-ray photoelectron spectroscopy.

Declarations

Ethics approval and consent to participate: Not applicable.

Consent for publication: All the data used for writing this manuscript has been cited with proper references.

Availability of data and materials: Data supporting the results are available in manuscript and can be supplied by the corresponding author on reasonable request.

Competing interests: The authors have no competing interests.

Funding: Not applicable

Authors' contributions: All authors had made equal contribution in collecting data, helping shape the manuscript and providing the critical feedback.

Sandeep Kumar: The corresponding author of this manuscript contributed via design and supervision of this work, data analysis and interpretation, wrote the manuscript with input from all authors.

Ravinderdeep Singh Brar: The author is research scholar in Department of Chemistry, Akal University and contributed via synthesis of nanocomposite material, and experimental data collection for the manuscript.

J Nagendra Babu: The author of this manuscript contributed via supervision of this work, data analysis and interpretation, providing critical feedback, discussion and writing this manuscript.

Amarjeet Dahiya: The author is research scholar in Department of Chemistry, Central University of Punjab and helped in experimental data collection for the manuscript.

Sandip Saha: The author of this manuscript contributed by data analysis and interpretation, designing the figures, providing critical feedback and helped shape the research writings.

Avneesh Kumar: The author helped in designing the work and providing critical feedback for the research outcomes.

Acknowledgements: The authors of this manuscript are thankful to Akal University for providing financial support and research facilities. We are also thankful to Central Instrumentation Facility, Central University of Punjab for assisting in physico-chemical characterization of the material.

Authors' information (optional)

References

Afroze S, Sen TK (2018) A review on heavy metal ions and dye adsorption from water by agricultural solid waste adsorbents. Water, Air, & Soil Pollution 229(7):1-50. https://doi.org/10.1007/s11270-018-3869-z

Aigberua A, Tarawou J, Abasi C (2018) Effect of oxidation-reduction fluctuations on metal mobility of speciated metals and arsenic in bottom sediments of middleton river, Bayelsa State, Nigeria. Journal of Applied Sciences and Environmental Management 22(9):1511-1517. https://doi.org/10.4314/jasem.v22i9.25.

Artioli Y (2008) Adsorption. In: Jørgensen SE, Fath BD (eds) Encyclopedia of Ecology. Academic Press, Oxford, p 60-65

Ashour EA, Tony MA (2020) Eco-friendly removal of hexavalent chromium from aqueous solution using natural clay mineral: activation and modification effects. SN Applied Sciences 2(12):1-13. https://doi.org/10.1007/s42452-020-03873-x

444 Banerjee M, Bar N, Basu RK, Das SK (2018) Removal of Cr (VI) from its aqueous solution using green adsorbent
445 pistachio shell: a fixed bed column study and GA-ANN modeling. Water Conservation Science and
446 Engineering 3(1):19-31. https://doi.org/10.1007/s41101-017-0039-x
447 Barceloux DG, Barceloux D (1999) Chromium. Journal of Toxicology: Clinical Toxicology 37(2):173-194.
448 https://doi.org/10.1081/CLT-100102418
449 Burrows D (2019) Chromium: metabolism and toxicity. CRC press
450 Carvalho FP (2017) Mining industry and sustainable development: time for change. Food and Energy Security
451 6(2):61-77. https://doi.org/10.1002/fes3.109.
452 Çelebi H (2020) Recovery of detox tea wastes: Usage as a lignocellulosic adsorbent in cr^{6+} adsorption. Journal of
453 Environmental Chemical Engineering 8(5):104310. https://doi.org/10.1016/j.jece.2020.104310
454 Chang P-H, Chou T-H, Sahu RS, Shih Y-h (2019) Chemical reduction-aided zerovalent copper nanoparticles for 2,
455 4-dichlorophenol removal. Applied Nanoscience 9(3):387-395. https://doi.org/10.1007/s13204-018-00945-
456 8
457 Cheng K, Winter WT, Stipanovic AJ (2012) A modulated-TGA approach to the kinetics of lignocellulosic biomass
458 pyrolysis/combustion. Polymer Degradation and Stability 97(9):1606-1615.
459 https://doi.org/10.1016/j.polymdegradstab.2012.06.027
460 Cottayil SK, Mohan M, Sivasubramanian G (2015) A simple, efficient and sustainable route to cellulose/cu
461 nanocomposite-evaluation of their antimicrobial and free radical scavenging activities. Journal of Green
462 Science and Technology 2(1):20-26. https://doi.org/10.1166/jgst.2015.1037
463 Crini G, Lichtfouse E (2019) Advantages and disadvantages of techniques used for wastewater treatment.
464 Environmental Chemistry Letters 17(1):145-155. https://doi.org/10.1007/s10311-018-0785-9
465 Devnani H, Rashid N, Ingole PP (2019) Copper/Cuprous oxide nanoparticles decorated reduced graphene oxide
466 sheets based platform for bio-electrochemical sensing of dopamine. ChemistrySelect 4(2):633-643.
467 https://doi.org/10.1002/slct.201803233
468 Dinh V-P, et al. (2020) Chitosan-MnO_2 nanocomposite for effective removal of Cr(VI) from aqueous solution.
469 Chemosphere 257:127147. https://doi.org/10.1016/j.chemosphere.2020.127147
470 Dong G, Ai Z, Zhang L (2014) Total aerobic destruction of azo contaminants with nanoscale zero-valent copper at
471 neutral pH: Promotion effect of in-situ generated carbon center radicals. Water research 66:22-30.
472 https://doi.org/10.1016/j.watres.2014.08.011
473 Garvey M (2019) Food pollution: a comprehensive review of chemical and biological sources of food contamination
474 and impact on human health. Nutrire 44(1):1-13. https://doi.org/10.1186/s41110-019-0096-3.
475 Gopinath KP, Madhav NV, Krishnan A, Malolan R, Rangarajan G (2020) Present applications of titanium dioxide
476 for the photocatalytic removal of pollutants from water: A review. Journal of Environmental Management
477 270:110906. https://doi.org/10.1016/j.jenvman.2020.110906
478 GracePavithra K, Jaikumar V, Kumar PS, SundarRajan P (2019) A review on cleaner strategies for chromium
479 industrial wastewater: present research and future perspective. Journal of Cleaner Production 228:580-593.
480 https://doi.org/10.1016/j.jclepro.2019.04.117

Guerra FD, Attia MF, Whitehead DC, Alexis F (2018) Nanotechnology for environmental remediation: materials and applications. Molecules 23(7):1760. https://dx.doi.org/10.3390%2Fmolecules23071760

He C, et al. (2020a) Cleaning chromium pollution in aquatic environments by bioremediation, photocatalytic remediation, electrochemical remediation and coupled remediation systems. Environmental Chemistry Letters 18(3):561-576. https://doi.org/10.1007/s10311-019-00960-3

He PY, Zhang YJ, Chen H, Han ZC, Liu LC (2020b) Low-cost and facile synthesis of geopolymer-zeolite composite membrane for chromium (VI) separation from aqueous solution. Journal of hazardous materials 392:122359. https://doi.org/10.1016/j.jhazmat.2020.122359

Hu X-j, et al. (2011) Adsorption of chromium (VI) by ethylenediamine-modified cross-linked magnetic chitosan resin: isotherms, kinetics and thermodynamics. Journal of hazardous materials 185(1):306-314. https://doi.org/10.1016/j.jhazmat.2010.09.034

Huang C-C, Lo S-L, Lien H-L (2012) Zero-valent copper nanoparticles for effective dechlorination of dichloromethane using sodium borohydride as a reductant. Chemical Engineering Journal 203:95-100. https://doi.org/10.1016/j.cej.2012.07.002

Iqbal J, et al. (2019) Synergistic effects of activated carbon and nano-zerovalent copper on the performance of hydroxyapatite-alginate beads for the removal of As^{3+} from aqueous solution. Journal of Cleaner Production 235:875-886. https://doi.org/10.1016/j.jclepro.2019.06.316

Ismail MIM (2020) Green synthesis and characterizations of copper nanoparticles. Materials Chemistry and Physics 240:122283. https://doi.org/10.1016/j.matchemphys.2019.122283

Ji C, Yin S-N, Sun S, Yang S (2018) An in situ mediator-free route to fabricate Cu_2O/g-C_3N_4 type-II heterojunctions for enhanced visible-light photocatalytic H_2 generation. Applied Surface Science 434:1224-1231. https://doi.org/10.1016/j.apsusc.2017.11.233

Jia T, Zhang B, Huang L, Wang S, Xu C (2019) Enhanced sequestration of Cr(VI) by copper doped sulfidated zerovalent iron (SZVI-Cu): Characterization, performance, and mechanisms. Chemical Engineering Journal 366:200-207. https://doi.org/10.1016/j.cej.2019.02.058

Jiang D, et al. (2018) Difunctional chitosan-stabilized Fe/Cu bimetallic nanoparticles for removal of hexavalent chromium wastewater. Science of The Total Environment 644:1181-1189. https://doi.org/10.1016/j.scitotenv.2018.06.367

Jorfi S, Ahmadi MJ, Pourfadakari S, Jaafarzadeh N, Soltani RDC, Akbari H (2017) Adsorption of Cr(VI) by natural clinoptilolite zeolite from aqueous solutions: isotherms and kinetics. Polish Journal of Chemical Technology 19(3):106-114. http://dx.doi.org/10.1515/pjct-2017-0056

Karimi-Maleh H, et al. (2020) Recent advances in removal techniques of Cr(VI) toxic ion from aqueous solution: A comprehensive review. Journal of Molecular Liquids:115062. https://doi.org/10.1016/j.molliq.2020.115062

Khan SU, Islam DT, Farooqi IH, Ayub S, Basheer F (2019) Hexavalent chromium removal in an electrocoagulation column reactor: Process optimization using CCD, adsorption kinetics and pH modulated sludge formation. Process Safety and Environmental Protection 122:118-130. https://doi.org/10.1016/j.psep.2018.11.024

517 Kullu B, Patra DK, Acharya S, Pradhan C, Patra HK (2020) AM fungi mediated bioaccumulation of hexavalent
518 chromium in Brachiaria mutica-a mycorrhizal phytoremediation approach. Chemosphere 258:127337.
519 https://doi.org/10.1016/j.chemosphere.2020.127337
520 Lace A, Ryan D, Bowkett M, Cleary J (2019) Chromium monitoring in water by colorimetry using optimised 1,5-
521 diphenylcarbazide method. International Journal of Environmental Research and Public Health
522 16(10):1803. https://dx.doi.org/10.3390%2Fijerph16101803
523 Le AT, Pung S-Y, Sreekantan S, Matsuda A (2019) Mechanisms of removal of heavy metal ions by ZnO particles.
524 Heliyon 5(4):e01440. https://doi.org/10.1016/j.heliyon.2019.e01440
525 Lei C, Wang C, Chen W, He M, Huang B (2020) Polyaniline@ magnetic chitosan nanomaterials for highly efficient
526 simultaneous adsorption and in-situ chemical reduction of hexavalent chromium: Removal efficacy and
527 mechanisms. Science of The Total Environment 733:139316.
528 https://doi.org/10.1016/j.scitotenv.2020.139316
529 Li B, et al. (2019) Facile modification of activated carbon with highly dispersed nano-sized α-Fe_2O_3 for enhanced
530 removal of hexavalent chromium from aqueous solutions. Chemosphere 224:220-227.
531 https://doi.org/10.1016/j.chemosphere.2019.02.121
532 Li C, Du Z, Zou W, Li H, Zhang C (2015a) Fabrication of copper coated polymer foam and their application for
533 hexavalent chromium removal. Reactive and Functional Polymers 88:24-30.
534 https://doi.org/10.1016/j.reactfunctpolym.2015.02.001
535 Li J, et al. (2018) Facile synthesis of Pd−Cu@Cu_2O/N-RGO hybrid and its application for electrochemical detection
536 of tryptophan. Electrochimica Acta 260:526-535. https://doi.org/10.1016/j.electacta.2017.12.125
537 Li P, Song Y, Wang S, Tao Z, Yu S, Liu Y (2015b) Enhanced decolorization of methyl orange using zero-valent
538 copper nanoparticles under assistance of hydrodynamic cavitation. Ultrasonics sonochemistry 22:132-138.
539 https://doi.org/10.1016/j.ultsonch.2014.05.025
540 Liu CF, et al. (2006) Physicochemical characterization of cellulose from perennial ryegrass leaves (Lolium perenne).
541 Carbohydrate Research 341(16):2677-2687. https://doi.org/10.1016/j.carres.2006.07.008
542 Lunk H-J (2015) Discovery, properties and applications of chromium and its compounds. ChemTexts 1(1):6.
543 https://doi.org/10.1007/s40828-015-0007-z
544 Mahmudi M, et al. (2020) An Alternative Activated Carbon from Agricultural Waste on Chromium Removal.
545 Journal of Ecological Engineering 21(8):1-9. https://doi.org/10.12911/22998993/127431
546 Mahringer D, Zerelli SS, Dippon U, Ruhl AS (2020) Pilot scale hexavalent chromium removal with reduction,
547 coagulation, filtration and biological iron oxidation. Separation and Purification Technology 253:117478.
548 https://doi.org/10.1016/j.seppur.2020.117478
549 Minas F, Chandravanshi BS, Leta S (2017) Chemical precipitation method for chromium removal and its recovery
550 from tannery wastewater in Ethiopia. Chemistry International 3(4):291-305.
551 https://doi.org/10.31221/osf.io/m7h5k

552 Mittal S, Vaid U, Nabi Najar G, Nagendra Babu J (2016) Removal of hexavalent chromium from aqueous solution:
553 a comparative study of cone biomass of “Picea smithiana” and activated charcoal. Desalination and Water
554 Treatment 57(24):11081-11095. https://doi.org/10.1080/19443994.2015.1038594
555 Mohamed MS, El-Arabi NI, El-Hussein A, El-Maaty SA, Abdelhadi AA (2020) Reduction of chromium-VI by
556 chromium-resistant Escherichia coli FACU: a prospective bacterium for bioremediation. Folia
557 microbiologica 65(4):687-696. https://doi.org/10.1007/s12223-020-00771-y
558 Namdar H, Akbari A, Yegani R, Roghani-Mamaqani H (2021) Influence of aspartic acid functionalized graphene
559 oxide presence in polyvinylchloride mixed matrix membranes on chromium removal from aqueous feed
560 containing humic acid. Journal of Environmental Chemical Engineering 9(1):104685.
561 https://doi.org/10.1016/j.jece.2020.104685
562 Nigam H, et al. (2015) Effect of chromium generated by solid waste of tannery and microbial degradation of
563 chromium to reduce its toxicity: a review. Adv Appl Sci Res 6(3):129-136.
564 Owlad M, Aroua MK, Daud WAW, Baroutian S (2009) Removal of hexavalent chromium-contaminated water and
565 wastewater: a review. Water, Air, and Soil Pollution 200(1):59-77. https://doi.org/10.1007/s11270-008-
566 9893-7
567 Pandey P, Saini VK (2019) Pillared interlayered clays: sustainable materials for pollution abatement. Environmental
568 Chemistry Letters 17(2):721-727. https://doi.org/10.1007/s10311-018-00826-0
569 Park J-Y, Jung Y-S, Cho J, Choi W-K (2006) Chemical reaction of sputtered Cu film with PI modified by low
570 energy reactive atomic beam. Applied Surface Science 252(16):5877-5891.
571 https://doi.org/10.1016/j.apsusc.2005.08.019
572 Patel H (2020) Batch and continuous fixed bed adsorption of heavy metals removal using activated charcoal from
573 neem (Azadirachta indica) leaf powder. Scientific Reports 10(1):1-12. https://doi.org/10.1038/s41598-020-
574 72583-6
575 Peng H, Guo J (2020) Removal of chromium from wastewater by membrane filtration, chemical precipitation, ion
576 exchange, adsorption electrocoagulation, electrochemical reduction, electrodialysis, electrodeionization,
577 photocatalysis and nanotechnology: a review. Environmental Chemistry Letters:1-14.
578 https://doi.org/10.1007/s10311-020-01058-x
579 Pradhan D, Sukla LB, Sawyer M, Rahman PK (2017) Recent bioreduction of hexavalent chromium in wastewater
580 treatment: a review. Journal of Industrial and Engineering Chemistry 55:1-20.
581 https://doi.org/10.1016/j.jiec.2017.06.040
582 Puszkarewicz A, Kaleta J (2019) Chromium (vi) adsorption on modified activated carbons. Applied Sciences
583 9(17):3549. https://doi.org/10.3390/app9173549
584 Qu J, et al. (2021) KOH-activated porous biochar with high specific surface area for adsorptive removal of
585 chromium (VI) and naphthalene from water: Affecting factors, mechanisms and reusability exploration.
586 Journal of Hazardous Materials 401:123292. https://doi.org/10.1016/j.jhazmat.2020.123292

Saraswathi MSSA, Nagendran A, Rana D (2019) Tailored polymer nanocomposite membranes based on carbon, metal oxide and silicon nanomaterials: a review. Journal of Materials Chemistry A 7(15):8723-8745. https://doi.org/10.1039/C8TA11460A

Shafizadeh F (1982) Introduction to pyrolysis of biomass. Journal of Analytical and Applied Pyrolysis 3(4):283-305. https://doi.org/10.1016/0165-2370(82)80017-X

Sharma AK, Devan RS, Arora M, Kumar R, Ma Y-R, Babu JN (2018) Reductive-co-precipitated cellulose immobilized zerovalent iron nanoparticles in ionic liquid/water for Cr (VI) adsorption. Cellulose 25(9):5259-5275. https://doi.org/10.1007/s10570-018-1932-y

Sharma AK, et al. (2015) In situ reductive regeneration of zerovalent iron nanoparticles immobilized on cellulose for atom efficient Cr (VI) adsorption. RSC advances 5(109):89441-89446. https://doi.org/10.1039/C5RA19917D

Sharma YC, Srivastava V, Weng CH, Upadhyay SN (2009) Removal of Cr(VI) from wastewater by adsorption on iron nanoparticles. The Canadian Journal of Chemical Engineering 87(6):921-929. https://doi.org/10.1002/cjce.20230

Shi L-n, Zhang X, Chen Z-l (2011) Removal of Chromium (VI) from wastewater using bentonite-supported nanoscale zero-valent iron. Water Research 45(2):886-892. https://doi.org/10.1016/j.watres.2010.09.025

Sperling M (2005) CHROMIUM. In: Worsfold P, Townshend A, Poole C (eds) Encyclopedia of Analytical Science (Second Edition). Elsevier, Oxford, p 113-126

Tadesse GL, Guya TK, Walabu M (2017) Impacts of tannery effluent on environments and human health: a review article. Advances in Life Science and Technology 54:10.

Turan NG, Mesci B (2011) Use of pistachio shells as an adsorbent for the removal of Zinc(II) ion. CLEAN – Soil, Air, Water 39(5):475-481. https://doi.org/10.1002/clen.201000297

Vaid U, Mittal S, Babu JN (2014) Removal of hexavalent chromium from aqueous solution using biomass derived fly ash from Waste-to-Energy power plant. Desalination and Water Treatment 52(40-42):7845-7855. https://doi.org/10.1080/19443994.2013.833554

Vardhan KH, Kumar PS, Panda RC (2019) A review on heavy metal pollution, toxicity and remedial measures: Current trends and future perspectives. Journal of Molecular Liquids 290:111197. https://doi.org/10.1016/j.molliq.2019.111197

Vilayatkar ND, et al. (2020) Synthesis and characterization of terpolymeric resin for removal of hexavalent chromium. Materials Today: Proceedings 29:776-780. https://doi.org/10.1016/j.matpr.2020.04.676

Wang H, Song X, Zhang H, Tan P, Kong F (2020) Removal of hexavalent chromium in dual-chamber microbial fuel cells separated by different ion-exchange membranes. Journal of hazardous materials 384:121459. https://doi.org/10.1016/j.jhazmat.2019.121459

Wang Y, Lü Y, Zhan W, Xie Z, Kuang Q, Zheng L (2015) Synthesis of porous Cu_2O/CuO cages using Cu-based metal–organic frameworks as templates and their gas-sensing properties. Journal of Materials Chemistry A 3(24):12796-12803. https://doi.org/10.1039/C5TA01108F

623 Wu S-J, Liou T-H, Mi F-L (2009) Synthesis of zero-valent copper-chitosan nanocomposites and their application for
624 treatment of hexavalent chromium. Bioresource technology 100(19):4348-4353.
625 https://doi.org/10.1016/j.biortech.2009.04.013
626 Xu D, Lv H, Liu B (2018a) Encapsulation of metal nanoparticle catalysts within mesoporous zeolites and their
627 enhanced catalytic performances: a review. Frontiers in chemistry 6:550.
628 https://doi.org/10.3389/fchem.2018.00550
629 Xu J, et al. (2018b) A review of functionalized carbon nanotubes and graphene for heavy metal adsorption from
630 water: Preparation, application, and mechanism. Chemosphere 195:351-364.
631 https://doi.org/10.1016/j.chemosphere.2017.12.061
632 Zakmout A, Sadi F, Portugal CA, Crespo JG, Velizarov S (2020) Tannery effluent treatment by nanofiltration,
633 reverse osmosis and chitosan modified membranes. Membranes 10(12):378.
634 https://doi.org/10.3390/membranes10120378
635 Zhang L, Song F, Wang S, Wang H, Yang W, Li Y (2020) Efficient removal of hexavalent chromium and congo red
636 by graphene oxide/silica nanosheets with multistage pores. Journal of Chemical & Engineering Data
637 65(9):4354-4368. https://doi.org/10.1021/acs.jced.0c00006
638 Zhao W, et al. (2019) Simultaneous removal of tetracycline and Cr(VI) by a novel three-dimensional AgI/BiVO4 p-
639 n junction photocatalyst and insight into the photocatalytic mechanism. Chemical Engineering Journal
640 369:716-725. https://doi.org/10.1016/j.cej.2019.03.115
641 Zhu F, Li L, Ma S, Shang Z (2016) Effect factors, kinetics and thermodynamics of remediation in the chromium
642 contaminated soils by nanoscale zero valent Fe/Cu bimetallic particles. Chemical Engineering Journal
643 302:663-669. https://doi.org/10.1016/j.cej.2016.05.072
644 Zhu F, Ma S, Liu T, Deng X (2018) Green synthesis of nano zero-valent iron/Cu by green tea to remove hexavalent
645 chromium from groundwater. Journal of Cleaner Production 174:184-190.
646 https://doi.org/10.1016/j.jclepro.2017.10.302

647

648

649

650

651

652

653

654

655

656

657

658

659

660

661

Figures

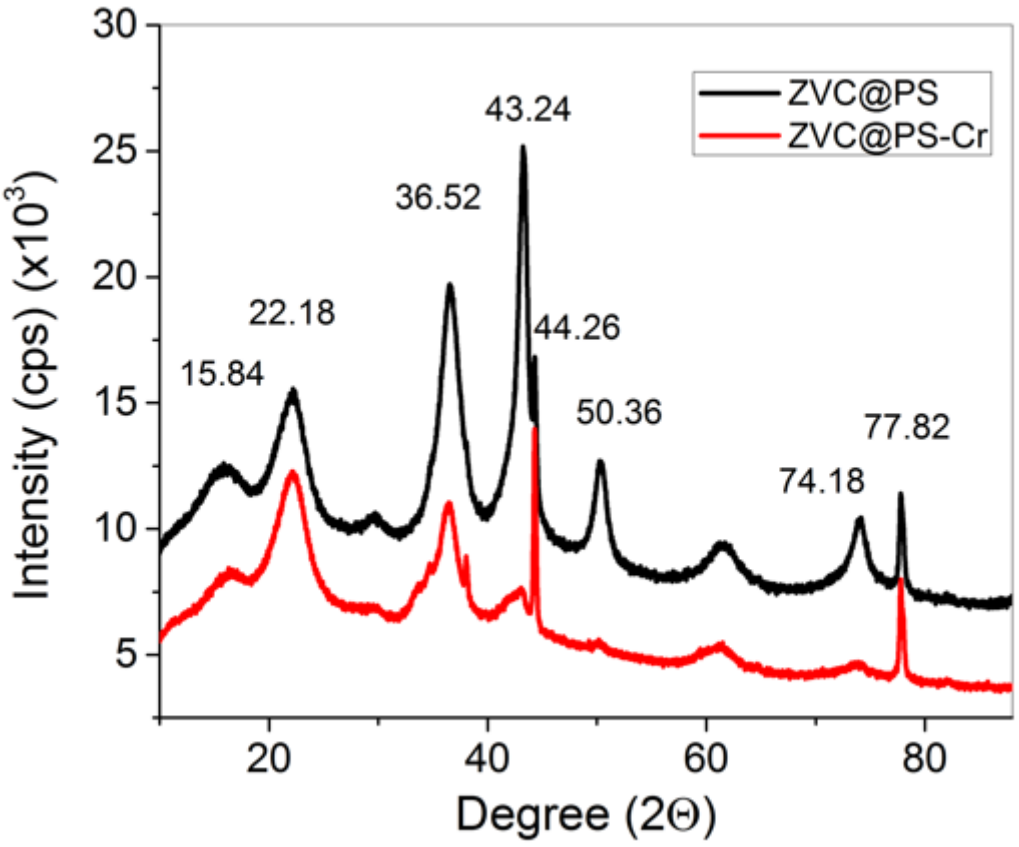

Figure 1

XRD pattern analysis of ZVC@PS and Cr(VI) adsorbed ZVC@PS samples

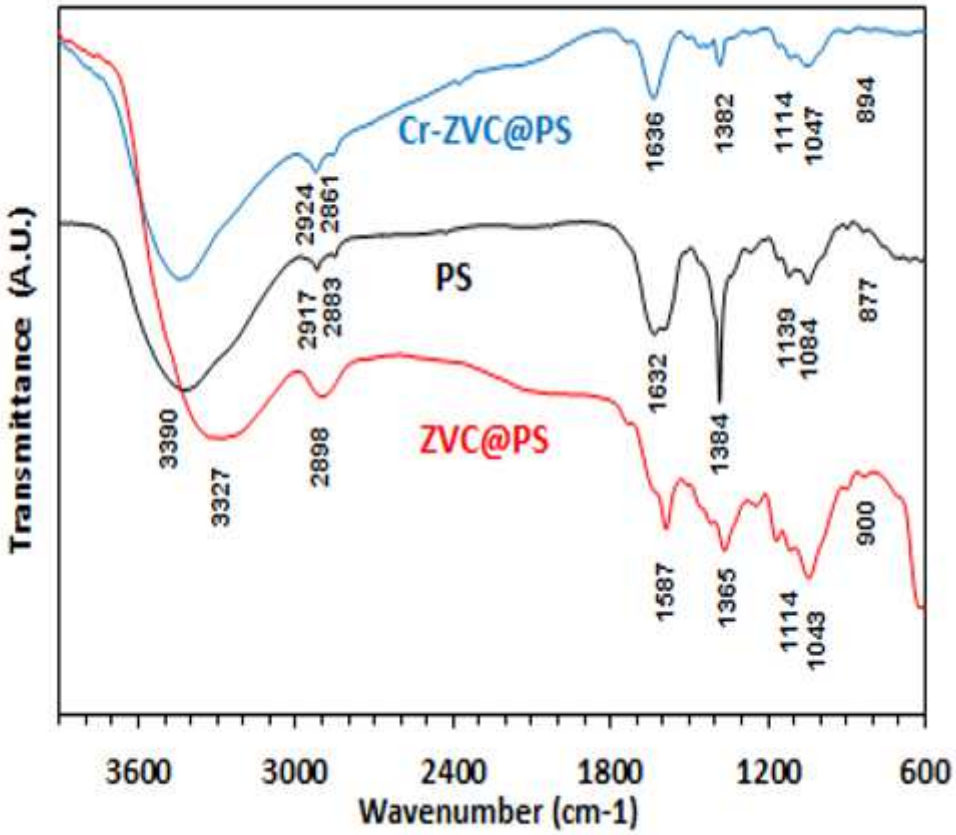

Figure 2

FTIR spectra of PS, ZVC@PS) and Cr(VI) adsorbed ZVC@PS samples

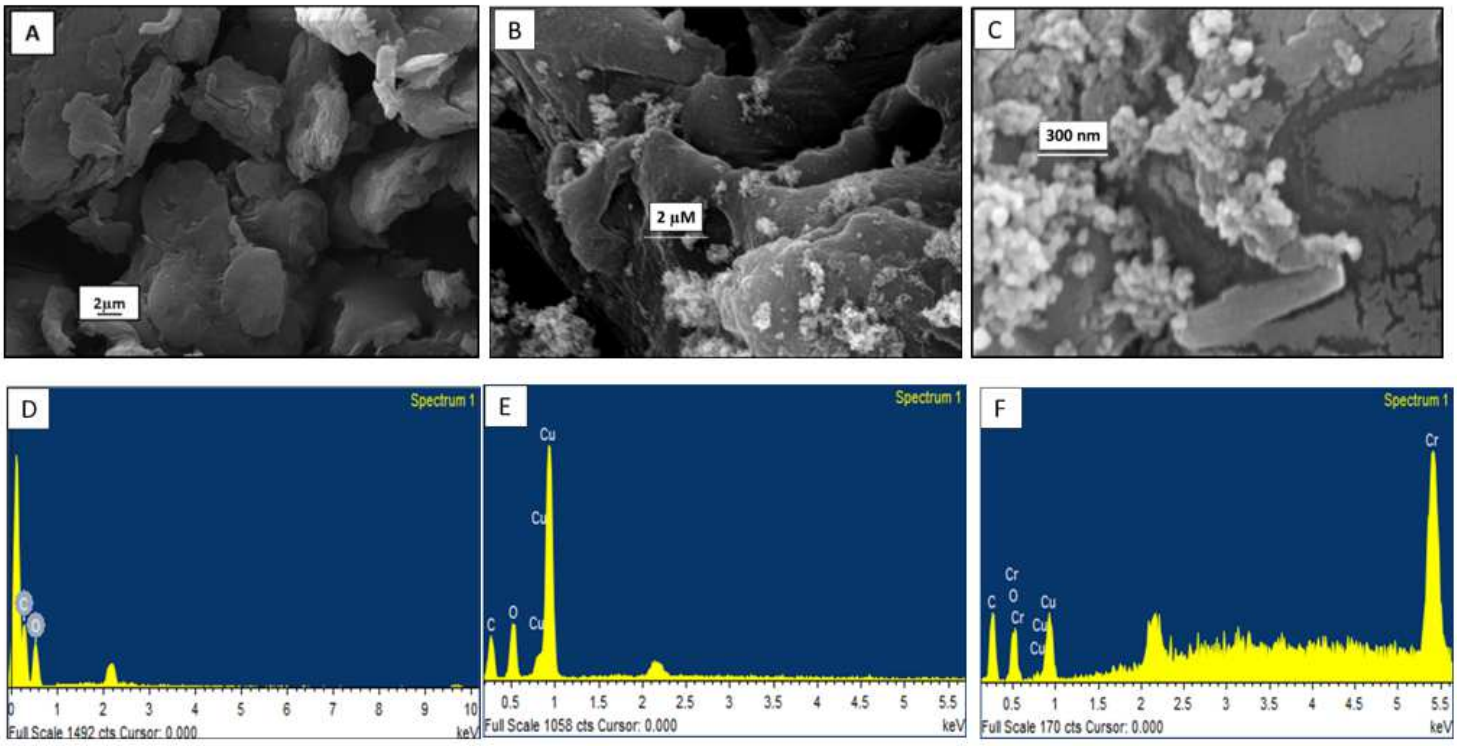

Figure 3

SEM images of (a) PS; (b) ZVC@PS; (c) ZVC@PS at increased magnification. EDX spectra of (d) PS; (e) ZVC@PS; and (f) Cr(VI) adsorbed ZVC@PS

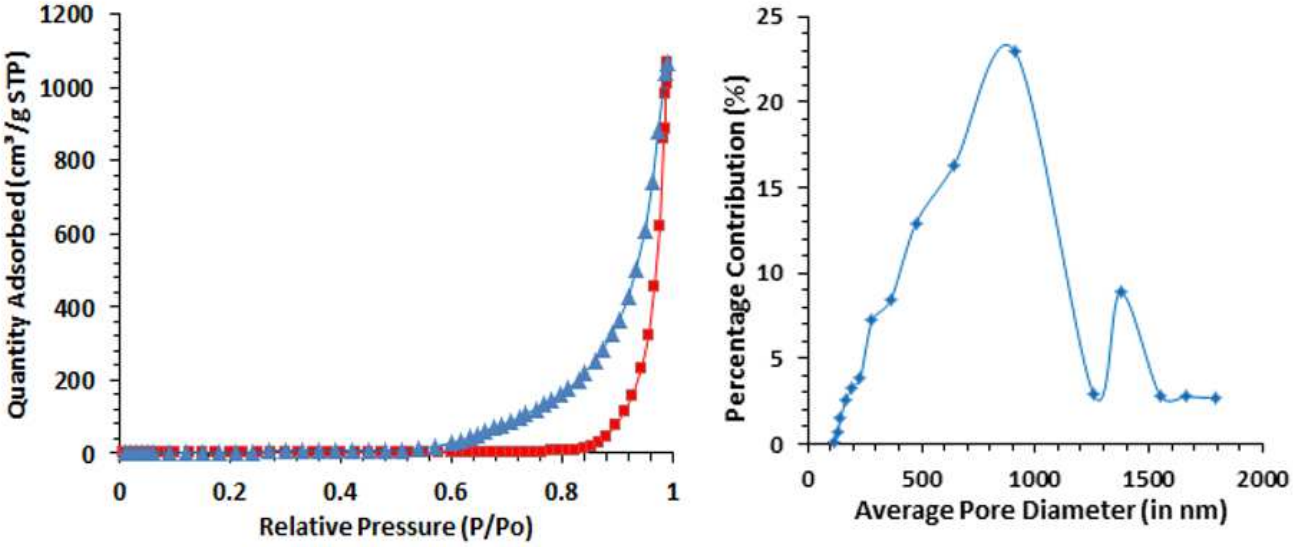

Figure 4

(a) Nitrogen adsorption-desorption isotherm for ZVC@PS; (b) average pore size distribution of ZVC@PS

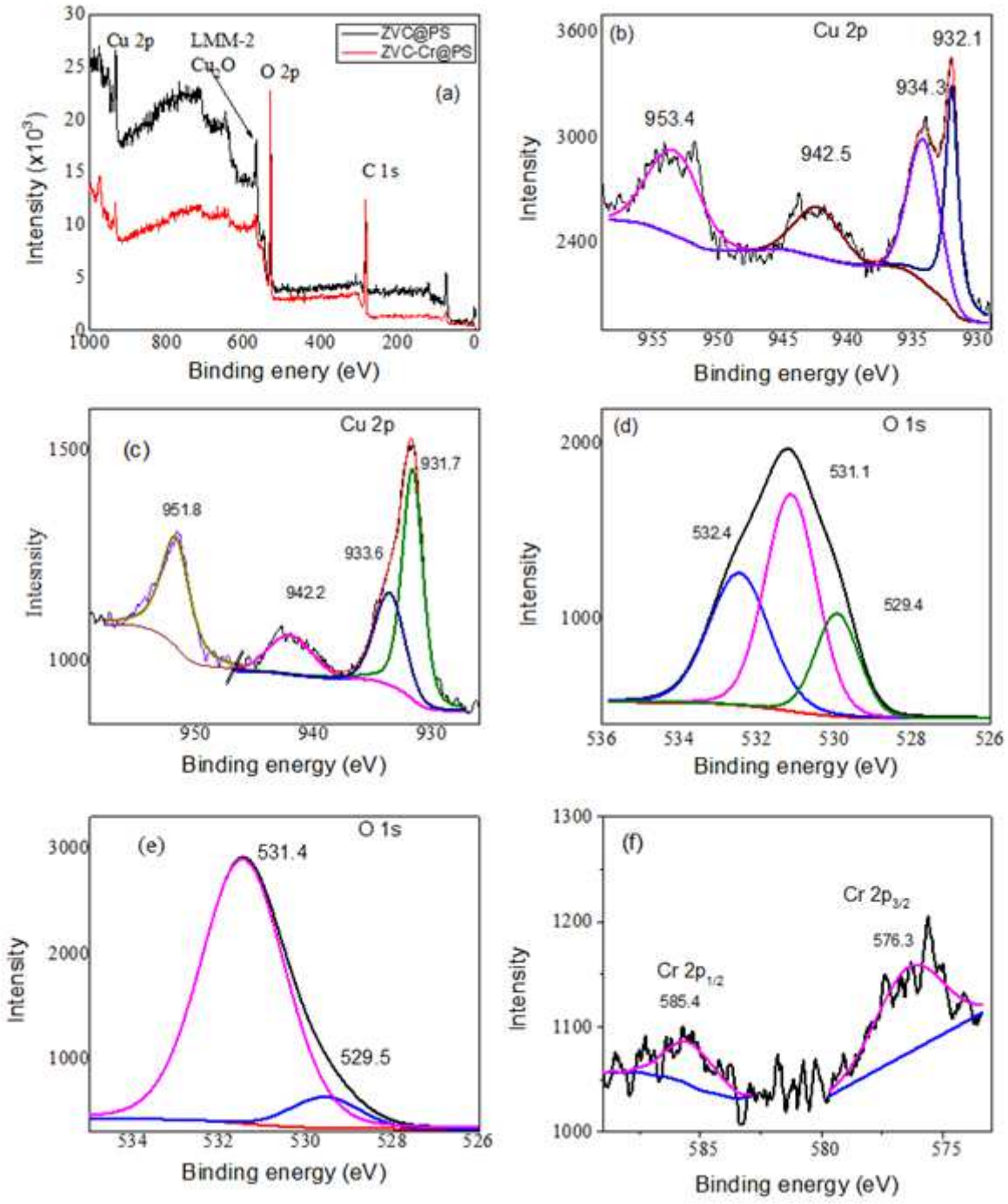

Figure 5

X-ray photoelectron spectroscopy spectra (a) survey scan of ZVC@PS; (b) Cu 2p before; and (c) Cu 2p after Cr(VI) adsorption on ZVC@PS; (d) O 1s before; and (e) O1s after Cr(VI) adsorption on ZVC@PS

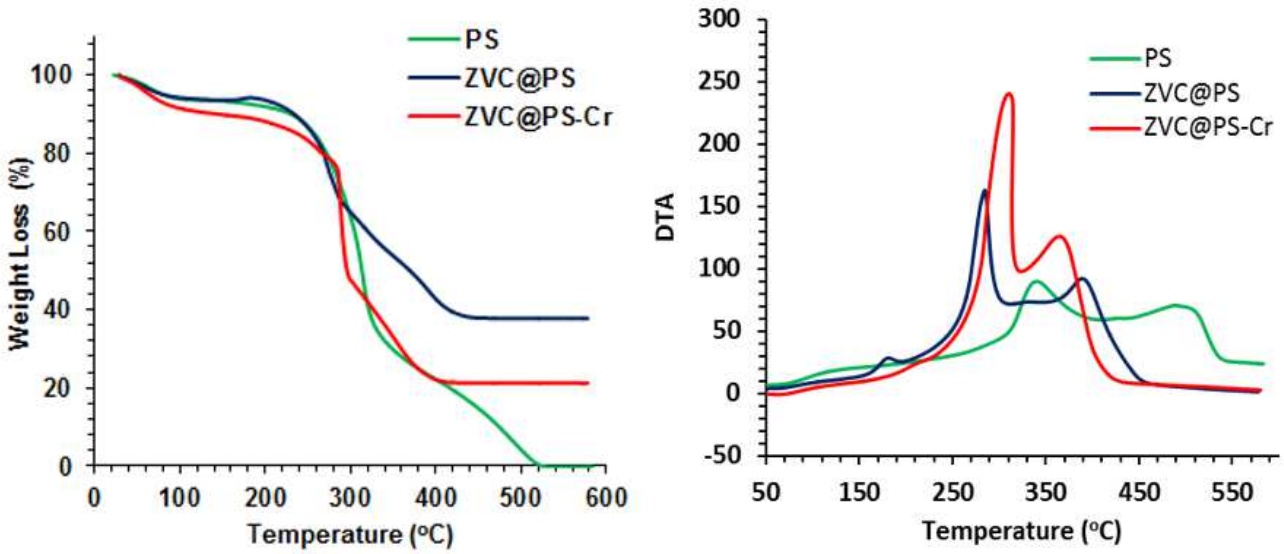

Figure 6

(a) TGA graphs; and (b) DTA curves of PS, ZVC@PS and ZVC@PS-Cr samples

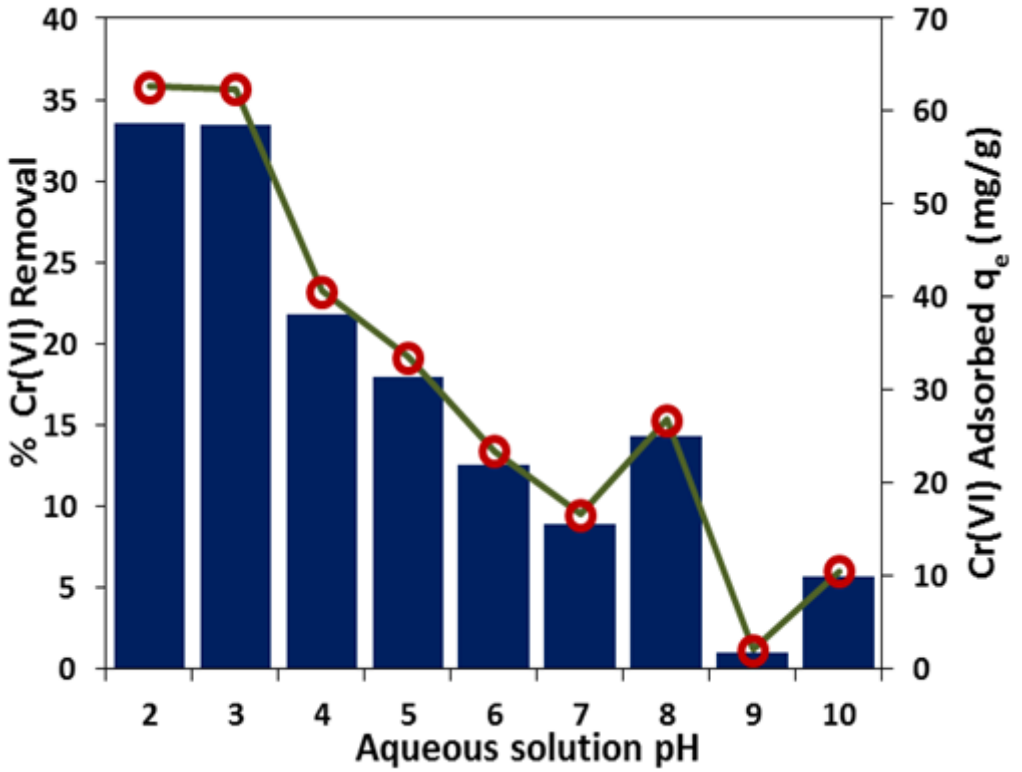

Figure 7

Effect of pH on Cr(VI) adsorption (qe) and % Cr(VI) removal efficiency of ZVC@PS. [When ZVC@PS dose is 100 mg/L, Cr(VI) concentration is 20 mg/L, contact time is 24 hours, and shaking speed is 200 RPM]

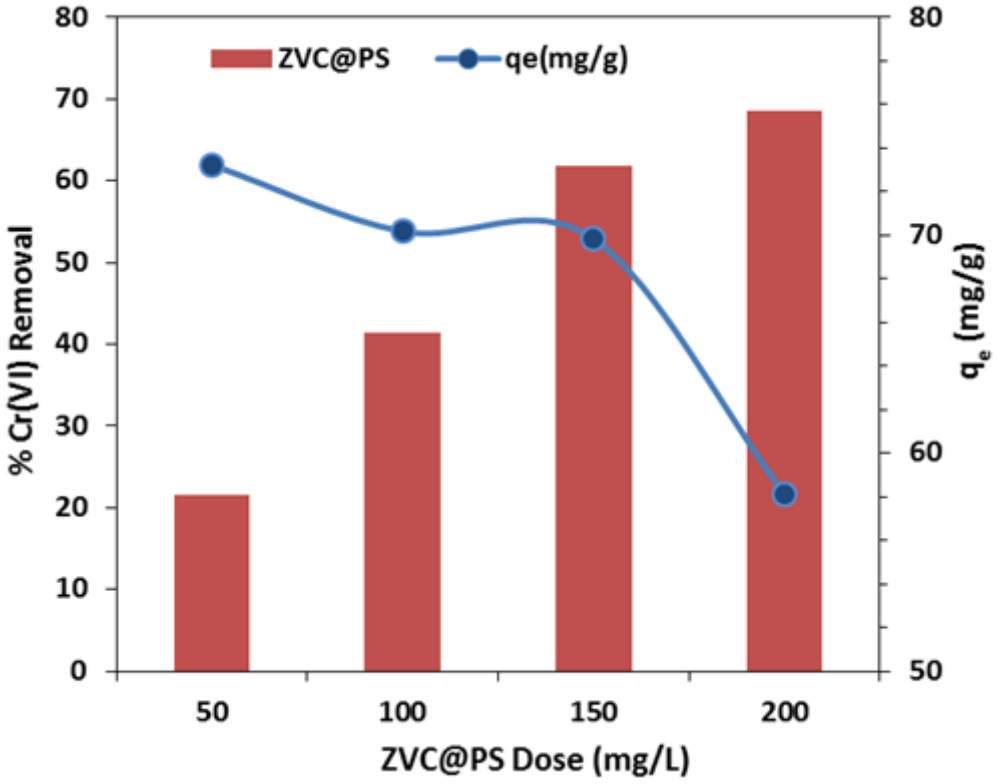

Figure 8

Effect of ZVC@PS dose concentration (50 to 200 mg/L) on Cr(VI) adsorption (qe) and % Cr(VI) removal, upon treatment with 20 mg/L of Cr(VI) solution at pH 3

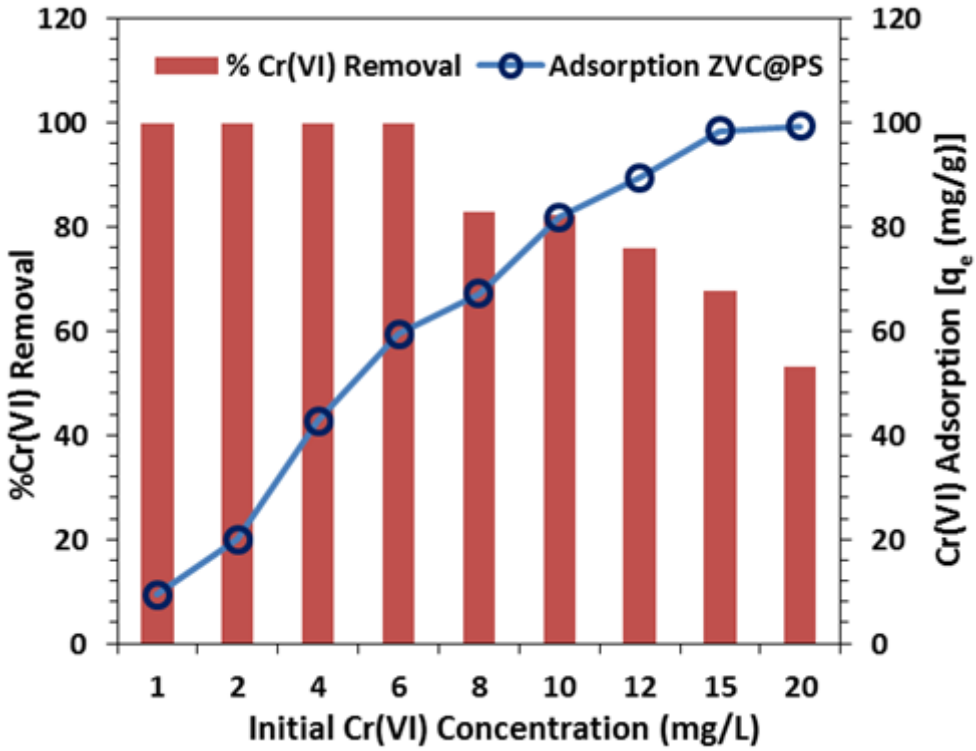

Figure 9

Effect of initial Cr(VI) concentration (1 to 20 mg/L) on Cr(VI) adsorption (qe) and % Cr(VI) removal efficiency of ZVC@PS

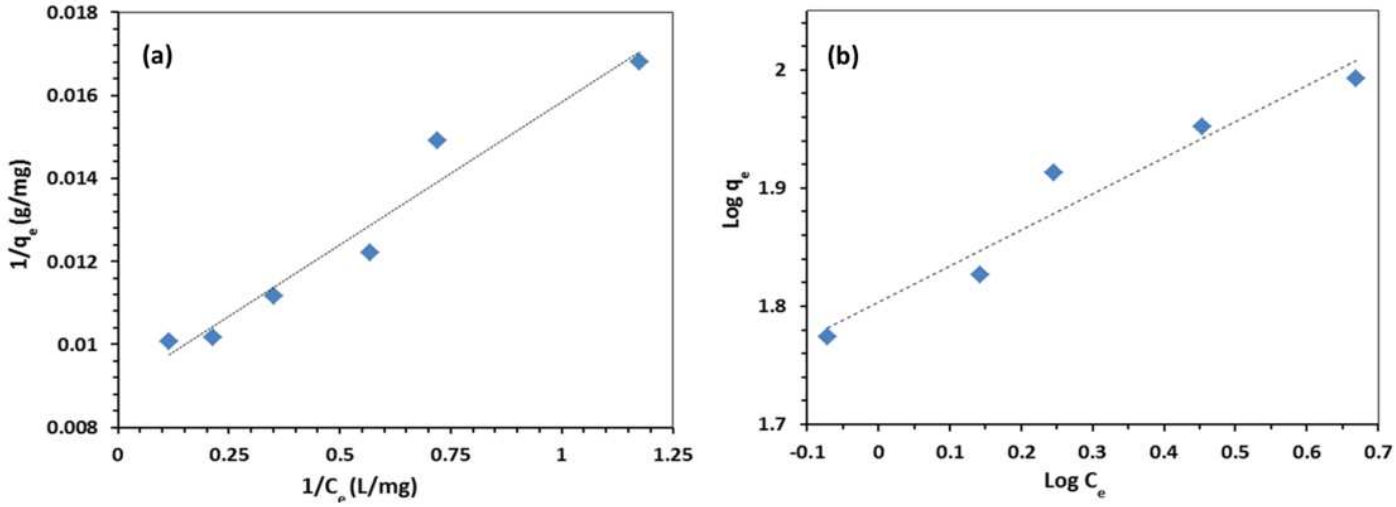

Figure 10

Langmuir adsorption isotherm (a); and Freundlich adsorption isotherm (b); for ZVC@PS for adsorption of Cr(VI)

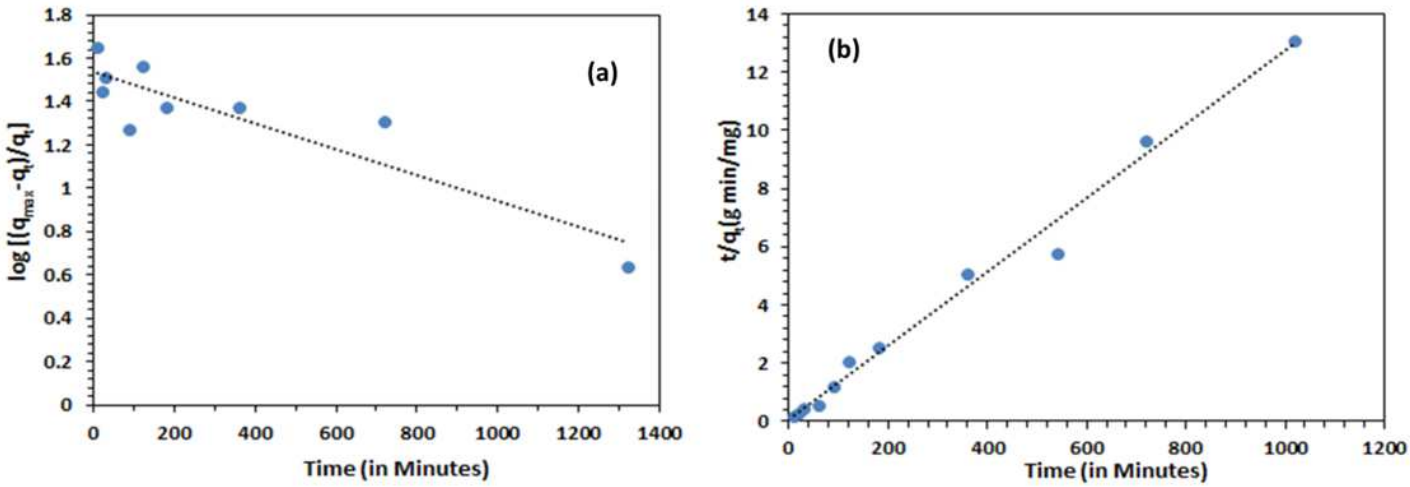

Figure 11

Linear fit plots of (a) pseudo first order and (b) pseudo second order adsorption kinetics

Supplementary Files

This is a list of supplementary files associated with this preprint. Click to download.

- GraphicalAbstarct.png